COMPARATIVE ANALYSES AND MODELLING FOR REGIONAL ECOSYSTEMS OF THE BLACK SEA

TÜLAY COKACAR, EMIN ÖZSOY

Institute of Marine Sciences, Middle East Technical University, P. O. Box 28, Erdemli, İçel 33731 Turkey

Abstract.

A zero dimensional ecosystem model is applied to the Black Sea to simulate the behaviour of its regional ecosystems. The modelling is guided by the analyses of the seasonal changes of mixed layer depth, nutrients and chlorophyll-a in the model regions, based on the available data in these areas of the Black Sea. Nutrients are continuously supplied to the adjacent coastal area by rivers, and in the other regions, mixed layer nutrient concentrations generally increase by mixing in winter. Despite the scarcity of data, it appears that the maximum chlorophyll-a concentration occurs in February-March in the central Black Sea, and in April-May in the peripheral regions, where the level is also an order of magnitude higher, as a result of riverine and coastal sources. The model successfully reproduces basic features of seasonal plankton and nutrient changes, and helps interpret the available observations and identify the factors creating the observed regional differences in productivity. The computed seasonal cycle of the chlorophyll-a compares well with the chlorophyll measurements in the central Black Sea. On the other hand, advection of nutrients is found to be important along the western and southern Black Sea coastal areas downstream of the river sources. Near the Bosphorus, reasonable agreement of model results and observations could only be ensured when the seasonal pattern of advection of river nutrients were taken into account. Better representation of the seasonal cycles including spring and autumn blooms are obtained with a nine compartment size fractionated model. Preliminary results are presented for a case including jelly organisms such as the ctenophore *Mnemiopsis leidyi*.

L.I. Ivanov and T. Oguz (eds.), Ecosystem Modeling as a Management Tool for the Black Sea, Vol. 2, 323-357.
© 1998 *Kluwer Academic Publishers. Printed in the Netherlands.*

1. Introduction

In the world ocean, as well as in the particular case of the Black Sea, the physical properties, circulation dynamics and mixing of the ambient waters are primary factors that influence the chemical and biological processes leading to marine productivity. The active circulation of the Black Sea redistributes physical properties and chemical constituents, and eddies and jets are believed to play important roles in the realization of primary productivity, and in the entrainment, recruitment and growth of various marine organisms (*e.g.* Sur *et al.*, 1994, 1996; Uysal and Sur, 1996). The study of mixing processes is essential in determining the sources and redistribution mechanisms of nutrients, the main factors of new production, and for understanding eutrophication processes and the distribution of organisms.

Our objective in the present study is to understand the dynamical behaviour of the lower trophic levels at different levels of model complexity including only first order physical effects, and to investigate the regional differences of the Black Sea ecosystem. A zero-dimensional ecosystem model after Fasham *et al.* (1990) is used to solve the time dependent coupled equations for the most essential system of biological and chemical elements. The model excludes any spatial dependence because it is obtained by vertically integrating the one-dimensional system of equations describing lower trophic level ecosystem dynamics within the mixed layer. The eventual goal of our studies is to construct box models corresponding to various modules of the Black Sea, coupled through fluxes, as guided by coarse resolution physical models.

2. Physical and Chemical Baseline Data

The model input data used in the present study were obtained from independent R/V Bilim cruises (1986-1995) of the IMS-METU (Institute of Marine Sciences), and the intercalibrated and pooled data sets obtained from joint cruises of ComsBlack programme (Aubrey *et al.*, 1992a,b; Oğuz *et al.*, 1993a,c; Konovalov *et al.*, 1994; Ivanov *et al.*, 1994) with the participation of the IMS-METU, the MHI (Marine Hydrological Institute) and the IBSS (Institute of Biology of Southern Seas) of Ukranie, and the RMRI (Romanian Marine Research Institute) of Romania. Nutrient data of the NATO TU - Black Sea Programme obtained after 1993 were kindly supplied by S. Konovalov of the MHI. Additional data were introduced from the hydrophysical data archives of Mamayev (1923-1992) and the data obtained from the Black Sea cruises of the R/V Knorr (1988 June-July). The mixed layer depth and the NO_3 concentration below the mixed layer obtained from these data were used as input parameters driving the model in specific regions.

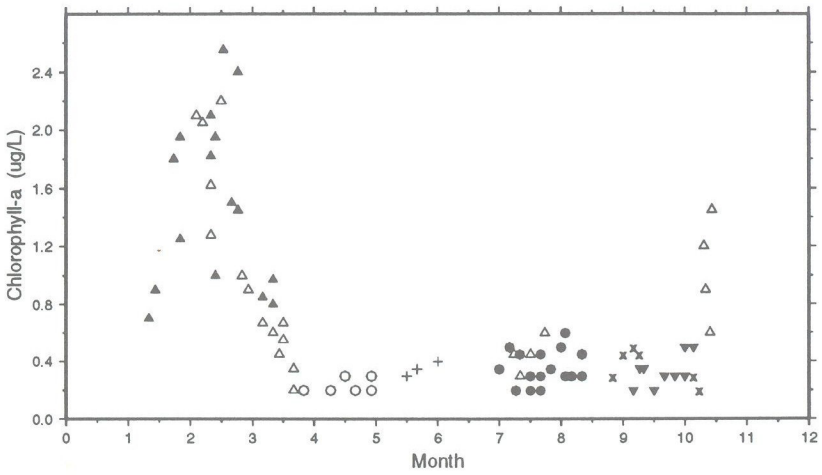


Figure 1. A composite picture of the euphotic layer average chlorophyll concentrations ($mg\ \mathrm{Chl-a}/m^3$) within a year in the central part of the Black Sea, compiled from different data sources (open and solid triangles: 1991; solid circles: 1989; open squares: 1988; plus signs: 1986; crosses:1985; open circles: 1984; solid reverse triangles: 1978). The data are redrawn from Vedernikov and Demidov (1993).

3. Validation Data

Unfortunately, there are only very few sources of data for comparison of the model results with observations, especially with regard to the biological variables such as primary production. The only sets of data available to us for comparison were mainly chlorophyll data assembled from the central part of the basin, and similar measurements near the northern entrance of the Bosphorus. Additionally, we compared mixed layer averages of nitrate, obtained from the above sets of measurements with those produced by the model.

The primary productivity and chlorophyll-a annual time series data indicate that the Black Sea exhibits characteristics of temperate basins with apparently two peaks observed during early spring and fall (Sorokin 1983; Vedernikov and Demidov, 1993). Figure 1 displays the annual cycle of chlorophyll-a within the central part of the basin, based on a synthesis of observations carried out during the last decade (Vedernikov and Demidov, 1993). The annual cycle of chlorophyll-a within the mixed layer in the vicinity of the Black Sea exit of the Bosphorus is displayed in Figure 2 within the northern exit region of Bosphorus, where time series of data were available (Chlorophyll-a measurements for stations K0 and B15 were kindly supplied to us by Çolpan Polat of the IMS-METU).

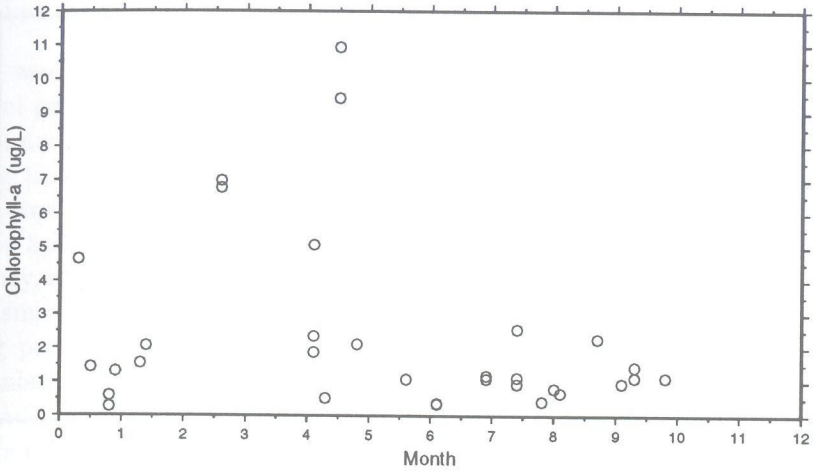


Figure 2. Seasonal composites of average Chlorophyll-a concentration ($mg\ Chl/m^3$) within the euphotic layer near the northern entrance of the Bosphorus (stations K0 and B15), unpublished data (Çolpan Polat, IMS-METU).

4. Identification of Model Regions in the Black Sea

Physical, biological and chemical properties of the Black Sea vary greatly on various spatial and temporal scales. However, it is possible to identify regions with specific characteristics of ecosystems. We divided the Black Sea basin into different model regions, based on these characteristics. Firstly, the Coastal Zone Colour Scanner data were used to qualitatively assess these characteristics. Accordingly, a basic difference in pigment concentrations along the western continental shelf / rim current zone and the interior regions, and secondly a gradual decrease along the periphery from the northwest shelf zone towards the south, where succession and changes in phytoplankton species occur. (USGOFSO, 1989; *e.g.* Sur *et al.*, 1994, 1996; ASRSOMS, 1996; Nezlin, 1997). Secondly, the topography of the shelf regions isolating the periphery from the interior were considered as a constraint, and circulation patterns obtained from numerical models were also used to identify the specific regions (*e.g.* Oğuz *et al.*, 1993, 1996; Trukhchev and Ibrayev, 1997).

The division of the basin into model regions was done on the basis of circulation represented by the computed dynamic anomalies from CTD surveys covering the entire area during the cruises between 1986-1995. Figure 3 shows the twelve model regions of the Black Sea, including the Danube river mouth and the Bosphorus sub-regions, added as specific regions with

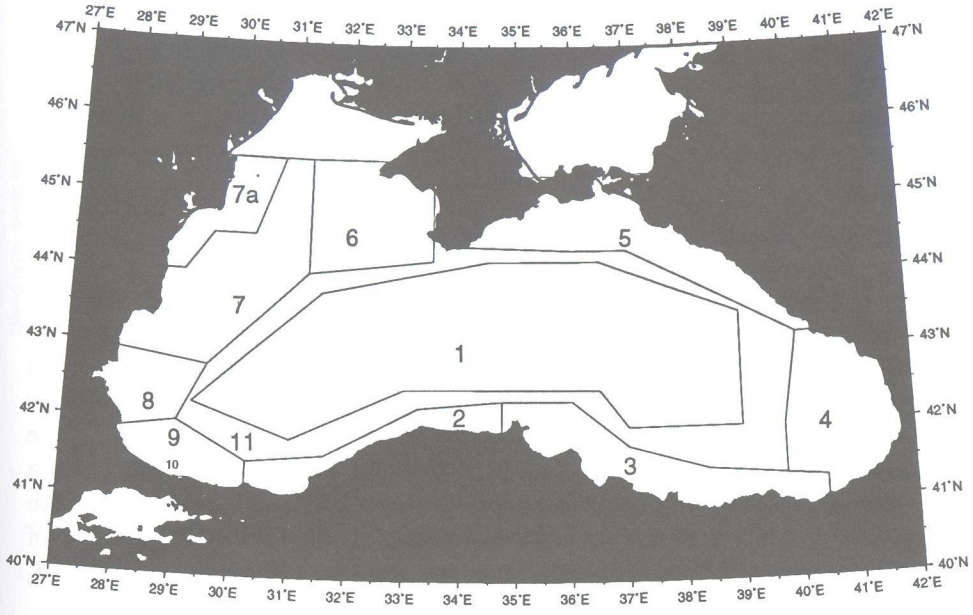


Figure 3. Geographic areas of the regional ecosystems of the Black Sea.

local characteristics. Ten regions were identified to have common features with respect to dynamic height anomalies. The regions with dynamic height anomaly $\leq -3\ cm$ were defined to be cyclonic (central), those with dynamic height anomaly $\geq 5\ cm$ to be anticyclonic (peripheral) regions, and those with dynamic height anomaly -3 to $5\ cm$ were assumed to correspond to the frontal zone of the rim current. In delineating the areas, mixed layer depth characteristics were also compared, and adjacent eddies with similar mixed layer depth changes in time were considered to belong together. The following characteristic regions (Figure 3) emerged from the above analyses: 1: central cyclonic gyre, 2: western Anatolian coast, 3: eastern Anatolian coast, 4: Batumi anticyclonic gyre, 5: Crimea-Caucasus, 6: Sevastopol anticyclonic eddy, 7: northwestern shelf, 7a: Danube estuary mouth, 8: Bulgarian coast, 9: Bosphorus shelf, 10: Bosphorus entrance, 11: Rim Current transition zone.

It is noteworthy that the division into regions 2 and 3 along the Anatolian coast is based on the differences in productivity between these regions (*e.g.* Sur *et al.*, 1994, 1996; Uysal and Sur 1995), despite the fact that these two regions are similar in terms of dynamic topography but different

in terms of mixed layer depth. A similar division into western and eastern parts could have been justified for the cyclonic central region, based on differences in primary productivity (*e.g.* USGOFSO, 1989; Hay *et al.*, 1991). Because of the smaller east-west differences in the central region in comparison to those amongst the coastal regions, and the lack of sufficient data, a single central region was defined.

5. Seasonal Variations of Mixed Layer Depth

Although a large volume of physical oceanographic measurements exist in the Black Sea, these are still not sufficient to reliably establish the climatological seasonal cycle of physical properties in all parts of the basin because of limited coverage in winter. When calculating the mixed layer depths for each region, the data from the recent cruises (1986-1995) were often insufficient, and therefore, bottle measurements of the Mamayev data set (1923-1992) were used to supplement the available information, despite the generally coarser sampling interval 5-10 m. The seasonal variation of average mixed layer depth for the analysed regions are given in Figure 4, with the 95 % confidence intervals marked with error bars.

6. Seasonal Variations of Nutrient Concentrations

Because the nutrient data are far less abundant than physical measurements, it is not possible to reconstruct the climatological seasonal pattern in all model regions. As a compromise, the regions are combined into larger groups to facilitate analyses. The depth and density dependent composite profiles of NO_3, PO_4, Si in the cyclonic region (1), the anticyclonic region (2, 3, 4, 5, 8, 9), the Danube estuary mouth region (7a), northwestern region (regions 6, 7) and the Bosphorus exit region (10) are plotted in Figures 5 and 6. Noise is evident in these nutrient measurements, and although the depth profiles in Figure 5 appear inconclusive, plots with respect to σ_θ density in Figure 6 leads to better characterisation of these regions.

The mixed layer NO_3 concentrations in the Danube and the Bosphorus regions (*Figure 5, panel D, E*) display high values. For the Danube region, the excess nutrients are introduced from the rivers. The Bosphorus exit region differs from the other regions by its two layer flow structure resulting from the exchange with the Mediterranean region and seems to receive coastal nutrients.

The composite profiles in Figure 5 are thus used to obtain model inputs for nutrient concentrations below the mixed layer and its rate of increase with density, used to supply the surface mixed layer by entrainment and mixing during mixed layer development.

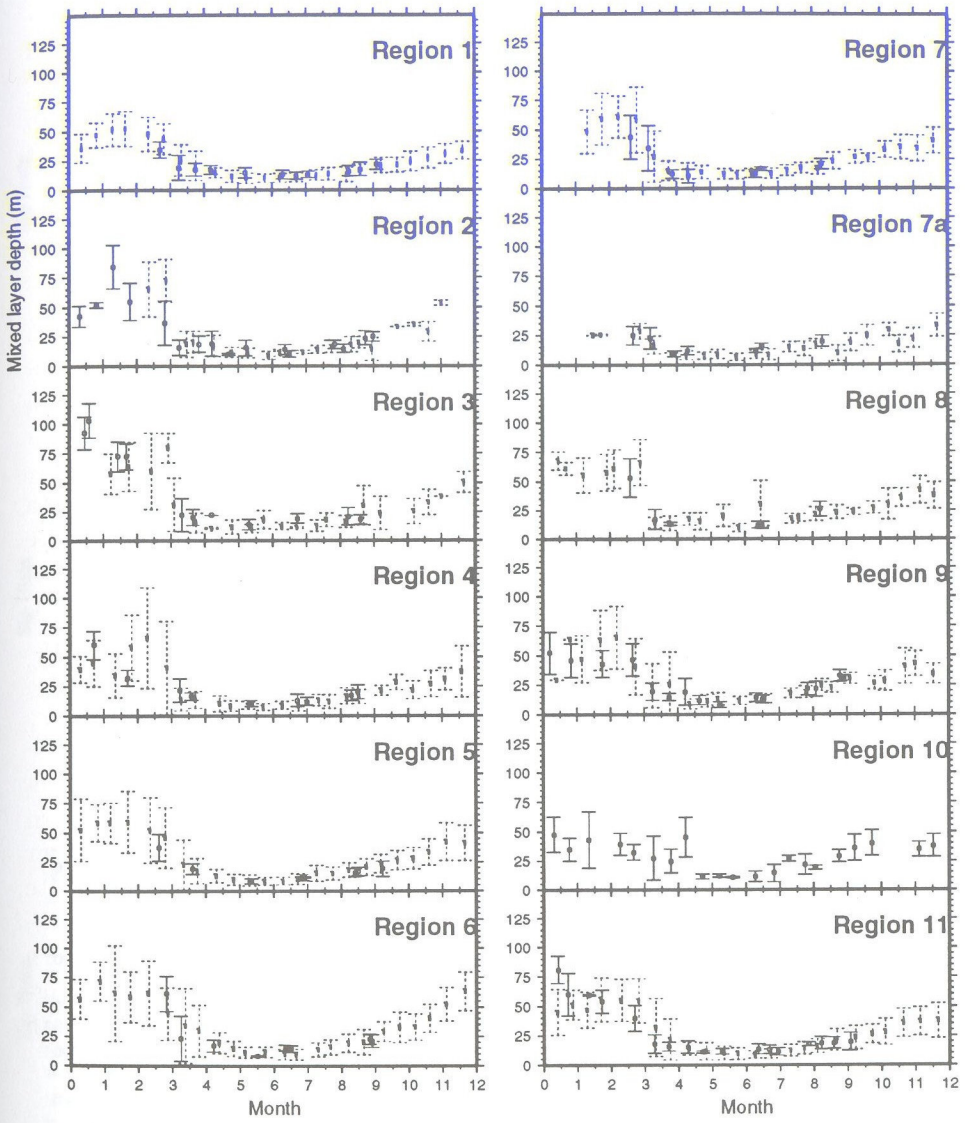


Figure 4. Seasonal variations of the average mixed layer depth in model regions, with 95% confidence limits marked by error bars; solid bars denote values obtained from the recent data base (1986-1995), while dashed bars denote values obtained from the Mamayev (1923-1992) data base.

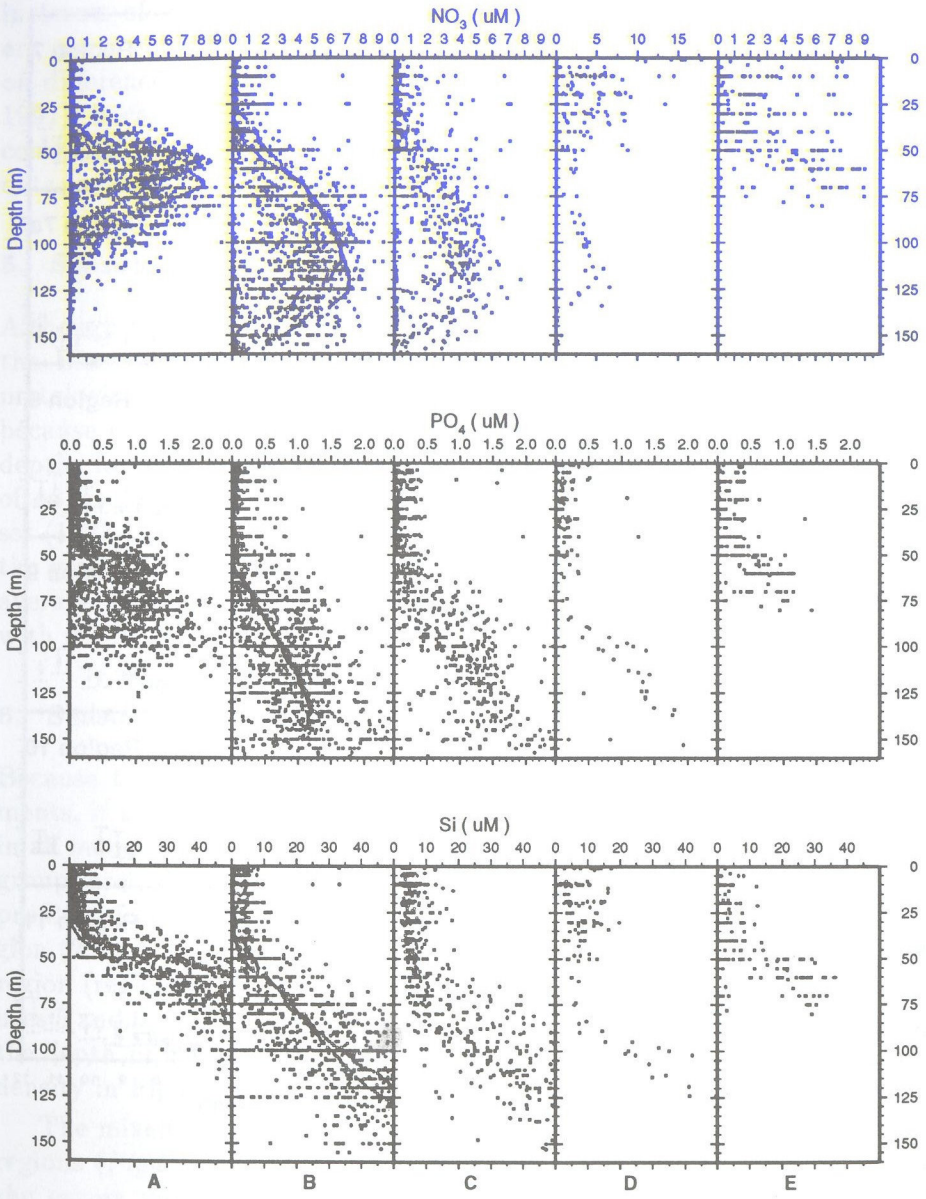


Figure 5. Variations of NO_3, PO_4 and Si concentrations (μM) with respect to depth in the (A) cyclonic region, (B) anticyclonic regions (C) northwestern region, (D) the Danube estuary mouth region, (E) Bosphorus exit region.

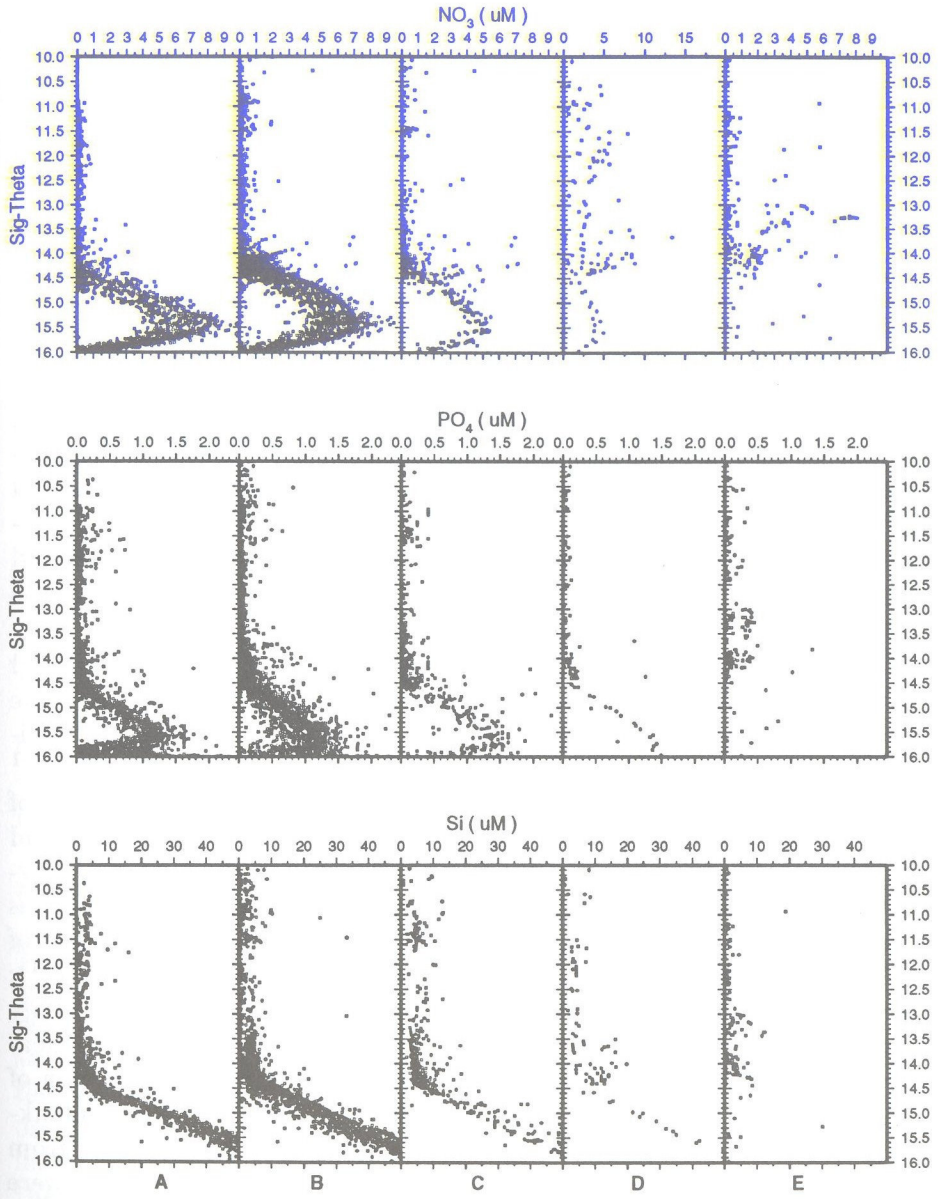


Figure 6. Variations of NO_3, PO_4 and Si concentrations (μM) with respect to density in the (A) cyclonic region, (B) anticyclonic regions (C) northwestern region, (D) the Danube estuary mouth region, (E) Bosphorus exit region.

The onset of increase in NO_3 and PO_4 in the cyclonic gyres appeared at greater density, but at shallower depths, in comparison with the anticyclonic regions including the north-west Black Sea. The sinking particulate organic matter (POM) in the anticyclonic regions therefore appears to have more time for remineralization. Other features of the nutrient distribution are in agreement with the analyses of Baştürk *et al.*, 1996.

7. Modelling

7.1. MODEL STRUCTURE AND CHOICE OF PARAMETERS

In the present study we use the ecological model developed by Fasham *et al.*, (1990), with several levels of internal organization including plankton, nutrients, detritus and bacterial production. The exchanges of matter, expressed in nitrogen units, are assumed to take place between the biological and chemical entities in the biologically active surface mixed layer. The inactive lower layer supplies nutrients to the mixed layer by entrainment and mixing. The system of equations are solved by fourth order Runge Kutta technique.

Model parameters specifically examined for the Black Sea are the mixed layer depth, light attenuation, sub-mixed layer nitrate, initial slope of the photosynthesis ($P-I$) curve, phytoplankton maximum growth rate, cloudiness and mixed layer temperature. We adjusted the values to $k_w = 0.08\ d^{-1}$ and $k_c = 0.02\ m^2\ (mMol\ N)^{-1}$ so as to produce a seasonal variation of $k_d = k_w + k_c P$ in the observed range of 0.1-0.2 in the central region, and varied them to match observed nutrient levels in the other regions. Phytoplankton maximum growth rates, based on in-situ data, were chosen as ($\gamma_p = 2 - 3\ d^{-1}$). The results were very sensitive to the initial slope of the $P - I$ curve: Values of α ranged within 0.049 - 0.094 $(Wm^{-2})^{-1}d^{-1}$); especially in regions influenced by river inputs, better results could only be obtained by adopting specific local values guided by some in-situ measurements. The other parameter values, such as the ammonium fraction of zooplankton excretion, the bacterial maximum growth rate, the zooplankton maximum growth rate, were mainly selected from the literature, from regions with conditions similar to the Black Sea. Where estimates were not available, parameter values were adopted from Fasham *et al.* (1990, 1994) and Ducklow and Fasham (1992), selecting reasonable ranges that best reproduced the available observations.

7.2. MODEL SIMULATIONS

In ecological modeling, the need for sufficient realism and that for simplification often compete. The level of complexity for the appropriate model had to be determined by considering the amount of available data, minimal groupings of biological functions and sizes *etc.* to obtain verifiable results.

7.2.1. *A 7-compartment Model (Phytoplankton, Zooplankton, Bacteria, DON, Nitrate, Ammonium, Detritus)*

The model with seven state variables including phytoplankton and zooplankton, bacteria, detritus, together with the nitrate, ammonia and DON fractions of nitrogen nutrients (P, Z, B, D, N_n, N_a, N_d), is described by Fasham *et al.* (1990).

The model was modified to include density dependent nitrate concentration below the mixed layer (see Table 2), determined with the help of data analyses. In Region 1, the model successfully reproduced the major observed features (Figure 7), only when realistic input parameters (first column of Table 1) and variable nutrients below the mixed layer were used together. Adjustments to model parameters were made in each of the other regions according to Table 2, to obtain representative results.

The spring bloom starts in the beginning of March and continues for more than a month, with a maximum value of 1.3 $mmol\ N\ m^{-3}$ (*Figure 8*). The model NO_3 concentrations within the mixed layer are close to the observed values, except in summer, when they tend to agree better with a subset of the observations obtained in the R/V Knorr experiments (Codispoti *et al.*, 1991).

7.2.2. *A 4-compartment (PZND) Model*

The 4-compartment $P - Z - D - N$ model (see Appendix) is obtained from the 7-compartment model, by combining nitrogen nutrients and bacteria into a single variable, *i.e.* $N = B + N_n + N_a + N_d$, and therefore would seem to be a good alternative to the 7-compartment model. Since the only terms dropped or simplified are those representing zooplankton grazing on bacteria and ammonia uptake, phytoplankton assimilation efficiency is increased (from 0.25 to 0.35) to establish equivalency. The runs made with the parameters of Table 3 are presented in Figure 9.

The model produces the correct magnitude of a phytoplankton bloom, but the timing of bloom is shifted by about 15 days relative 7-compartment case, as a result of the slightly different nutrient limitation function used. Because the reduced model excludes the NH_4 compartment, the nitrogen limitation is altered, with lower nutrient availability in winter (*Figure 9*), resulting in higher nitrogen concentration in summer, forced by zooplankton excretion and phytoplankton exudation.

TABLE 1. 7-compartment model parameters common for all regions

Parameter	*Symbol*	*Units*	*Value*	*Oğuz*
Mixed layer depth	h	m		
Diffusive mixing rate	m	$m\ d^{-1}$	0.1	
PAR/total irradiance	-		0.41	
Cloudiness	-	*oktas*	4	
Light attenuation by water	k_w	m^{-1}	(Table 2)	0.08
Phytop. max. growth rate	γ_p	d^{-1}	(Table 2)	1.5
Initial slope of $P-I$ curve	α	$(W\ m^{-2})^{-1}d^{-1}$	(Table 2)	0.01
Half-sat., for NO_3^- uptake by P	K_{pn}	$mmol\ N\ m^{-3}$	0.5	0.5
Half-sat., for NH_4^+ uptake by P	K_{pa}	$mmol\ N\ m^{-3}$	0.2	0.2
Phytop. specitic mortality rate	μ_p	d^{-1}	0.045	0.04
Light atten. by phytoplankton	k_c	$m^2(mmol\ N)^{-1}$	0.02	0.07
Phytop. exudation fraction	e		0.05	
NH_4^+ inhibition parameter of P	Ψ_a	$(mmol\ N)^{-1}$	1.5	
Zooplankton max. growh rate	γ_z	d^{-1}	(see Table 1b)	0.8
Zoop. ass. eff. feeding on P, B, D	β_p,β_b,β_d		0.75	0.75
Zoop. spec. excretion rate	ν_z	d^{-1}	0.1	0.07
Zoop. spec. mortality rate	μ_z	d^{-1}	0.05	0.04
Zoop. half-sat. for ingestion	K_z	$mmol\ N\ m^{-3}$	1.0	0.5
Detrital frac. of Zoop. mortality	d		0.33	
NH_4^+ frac. of Zoop. excretion	a		0.75	
Bacterial max. growth rate	γ_b	d^{-1}	0.5	
Bacterial specific excretion rate	ν_b	d^{-1}	0.05	
Bacterial Half-sat.rate for uptake	K_b	$mmol\ N\ m^{-3}$	0.5	
NH_4^+ / DON uptake ratio	η		0.6	
Detrital breakdown rate	μ_d	d^{-1}	0.05	0.01
Detrital sinking rate	w_d	$m\ d^{-1}$	1.0	1.0

growth and mortality rates. The grazing effect of *Mnemiopsis* on zooplakton caused a break in the bloom in winter time. Decreasing pressure on phytoplankton by its consumer zooplankton, consumed in turn by *Mnemiopsis*, caused an increase in the phytoplankton biomass in April. In addition, the bacterial biomass was increased considerebly in comparison to the previous runs because of their mucus uptake.

Contrary to observed summer time increase in the mnemiopsis biomass within the interior of the basin, the model provided a late spring - early summer increase in response to the increasing zooplankton biomass, and a delayed phytoplankton bloom. Improvements in understanding of the basic Mnemiopsis behaviour in terms of selective feeding, growth and decay

TABLE 2. 7-compartment model parameters for specific regions

region	k_w	γ_p	α	γ_z	z_c	S	y_d
1	0.08	2.5	0.17	1.3	18	0.14	0.3
2	0.08	2.5	0.03	1.5	25	0.08	0.4
3	0.1	2.5	0.04	1.8	25	0.05	0.4
4	0.08	2.5	0.025	2	25	0.07	0.4
5	0.08	2.5	0.03	1.8	25	0.07	0.4
6	0.08	2.5	0.03	1.7	25	0.04	0.4
7	0.1	2.	0.04	1.8	25	0.04	0.4
7a	0.18	2.5	0.03	1.5	10	0.1	2
8	0.1	2.	0.04	1.8	25	0.07	0.4
9	0.1	2.5	0.04	2	25	0.07	0.4
10	0.12	2.5	0.04	1	25	0.2	0.5
11	0.1	2.5	0.04	1.8	25	0.07	0.4

nutrients below the mixed layer modelled by:
$y_m = y_d,\ z < z_c$
$y_m = y_d + S(z - z_c),\ z \geq z_c$

processes could lead to better forecasts in the future.

7.2.4. *A 9-compartment Model (Size Classification of Phytoplankton and Zooplankton)*

A model with 9-compartments including size speciation is constructed, as described in Table 5 and the Appendix. This is similar to the 7-compartment model, but now 2 size-classes each of phytoplankton and zooplankton are included. The two size-classes of the phytoplankton roughly correspond to a division between net-phytoplankton (mainly diatoms) P_1, and pico-phytoplankton (other species) of phytoplankton P_2. The P_1 phytoplankton have a maximum growth rate which is larger than the P_2 phytoplankton, and also have a large sinking rate, while the sinking rate for the P_2 phytoplankton could be neglected. The growth rate of P_1 phytoplankton (diatoms) is also usually larger.

Similarly, the zooplankton can be divided into two large sub-groups, namely the meso-zooplankton (mainly copepods) Z_1 that typically make up about 80 % of the total zooplankton biomass, and micro-zooplankton (mainly ciliates or protozoa) Z_2, which make up about 20 % of the zooplankton in the Black Sea. In the model, following Ducklow and Fasham (1992), it is assumed that Z_1 consumes P_1, Z_2 and D, while Z_2 consumes P_2, B and D. Both size classes of zooplankton produce fecal products, but

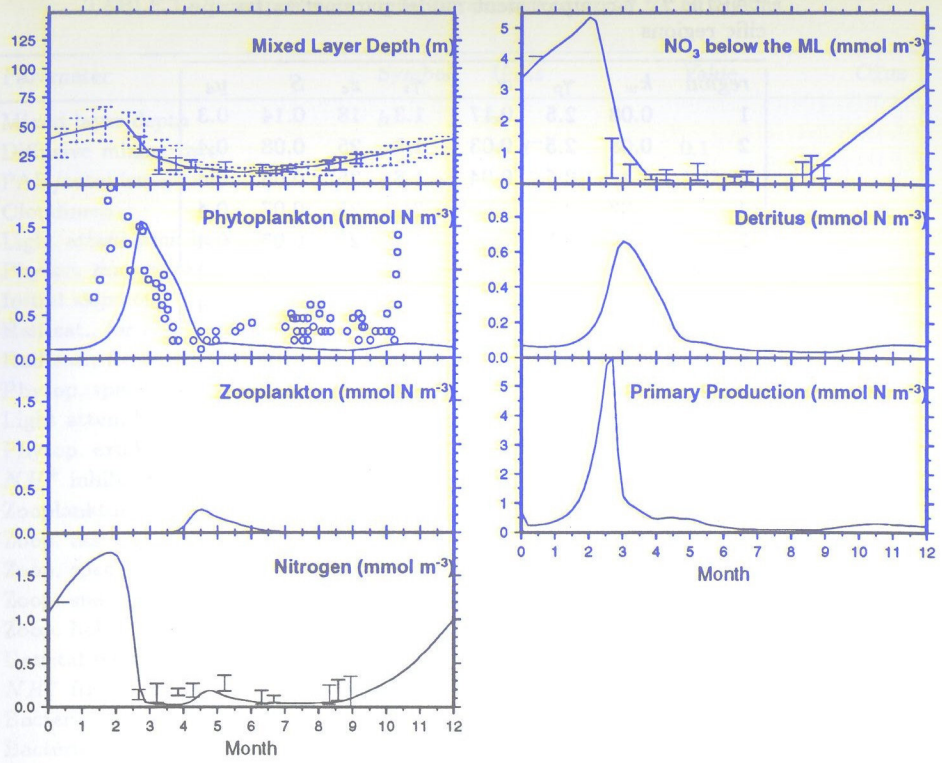


Figure 9. Results of the 4-compartment model, run with values of constants in Table 3 for region 1 (nutrient bars show NO_3).

it is assumed that the mesozooplankton pellets have fast sinking rates, so as to sediment out of the mixed layer before any significant re-ingestion can take place. In contrast, the microzooplankton fecal pellets are assumed to sink slowly to form part of the euphotic zone detritus capable of being reingested by both size classes of zooplankton.

The behaviour of the model is sensitively dependent on light, grazing, and mortality parameters, while it is less dependent on the growth parameters. Within a large range of parameters, this model gives stable results in producing a pico-phytoplankton bloom P_2 in the winter periods, replaced by a sustained high level of net-phytoplankton P_1 in spring, and late autumn bloom of P_2 as shown in Figure 11. This pattern may be reminescent of the continuous blooms of dinoflagellates in summer. The meso-zooplankton Z_1 biomass increase during March-April and as a result of their grazing the bacterial biomass decreases. Following the Z_2 depletion as a result of Z_1 consumption, the bacterial biomass increases once again. In this simulation,

TABLE 3. 4-compartment model parameters

Parameter	*Symbol*	*Units*	*Value*
Mixed layer depth	h	m	
Diffusive mixing rate	m	$m\ d^{-1}$	0.1
PAR/total irradiance	-		0.41
Cloudiness	-	*oktas*	4
Light attenuation caused by water	k_w	m^{-1}	0.08
Phytoplankton maximum growth rate	γ_p	d^{-1}	2.5
Initial slope of $P-I$ curve	α	$(W\ m^{-2})^{-1}d^{-1}$	0.017
Half-sat., for nitrogen uptake by P	K_{pn}	$mmol\ N\ m^{-3}$	0.5
Phytop. specific mortality rate	μ_p	d^{-1}	0.045
Light atten. by phytoplankton	k_c	$m^2(mmol\ N)^{-1}$	0.03
Phytop. exudation fraction	e		0.05
Zooplankton maximum growh rate	γ_z	d^{-1}	2.2
Zoop. ass. eff. feeding on P	β_p		0.35
Zoop. ass. eff. feeding on D	β_d		0.25
Zoop. spec. excretion rate	ν_z	d^{-1}	0.1
Zoop. spec. mortality rate	μ_z	d^{-1}	0.05
Zoop. half-sat. for ingestion	K_z	$mmol\ N\ m^{-3}$	1.0
Detrital fraction of Zoop. mortality	d		0.33
Detrital breakdown rate	μ_d	d^{-1}	0.05
Detrital sinking rate	w_d	$m\ d^{-1}$	1.0

the Z_2 grazing reduced the P_2 biomass to a low level before the nutrients were exhausted from zooplankton regeneration and mixing was sufficient to meet the demands of P_1 growth. In fact, Z_2 is present in the system when the P_1 bloom occurs, because of its preferential grazing on P_2, so that the bloom continues till the Z_1 biomass increases in the system.

7.2.5. *Model Comparisons and Sensitivity Analyses*

The simple four compartment model results in realistic simulations of the qualitative features of the seasonal production cycle. The $P-Z-D-N$ model has the advantage of simplicity but better results are obtained when more complexity is invoked with the 7-compartment model. Better representation of the the seasonal cycles including spring and autumn blooms (compare Figures 8 and 11) are obtained with a 9-compartment model with size classes.

The performance of model run with Mnemiopsis was not satisfactory for the Black Sea. The observations of Mnemiopsis biomass for the central Black Sea show increases in summer. The model gave a late spring

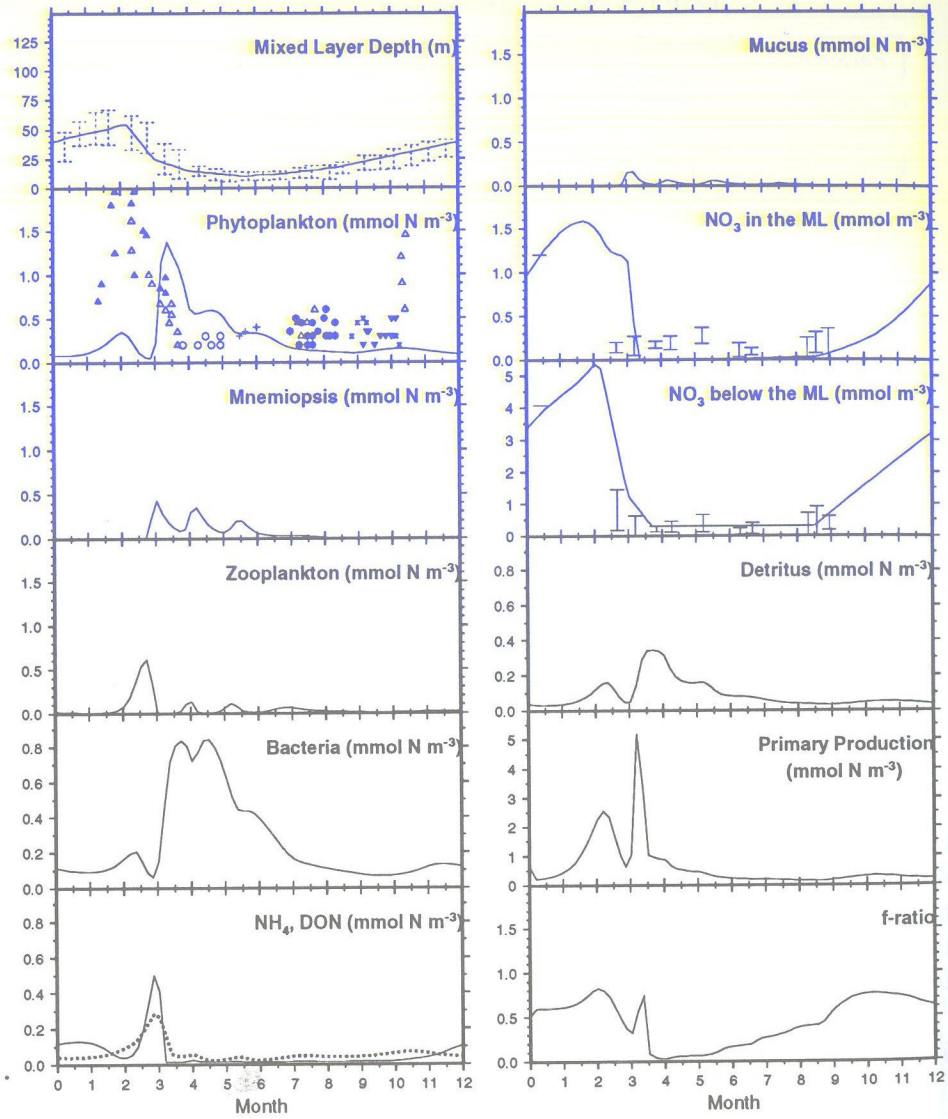


Figure 10. Results of model including Mnemiopsis, run with values of constants in Table 4 for region 1.

increase, in response to the increasing zooplankton biomass, and a delayed phytoplankton bloom.

A sub-group of the 27 parameters used in the 7-compartment model and the mixed layer depth, cross-pycnocline mixing rate and the sub-pycnocline

TABLE 4. 9-compartment (Mnemiopsis, mucus) model parameters

Parameter	*Symbol*	*Units*	*Value*
Mixed layer depth	h	m	
Diffusive mixing rate	m	$m\ d^{-1}$	0.1
PAR/total irradiance	-		0.41
Cloudiness	-	*oktas*	4
Light attenuation caused by water	k_w	m^{-1}	0.08
Phytoplankton maximum growth rate	γ_p	d^{-1}	2.5
Initial slope of $P-I$ curve	α	$(W\ m^{-2})^{-1}d^{-1}$	0.017
Half-sat., for NO_3^- uptake by P	K_{pn}	$mmol\ N\ m^{-3}$	0.5
Half-sat., for NH_4^+ uptake by P	K_{pa}	$mmol\ N\ m^{-3}$	0.5
Phytop. specitic mortality rate	μ_p	d^{-1}	0.045
Light atten. by phytoplankton	k_c	$m^2(mmol\ N)^{-1}$	0.03
Phytop. exudation fraction	e		0.05
NH_4^+ inhibition parameter of P	Ψ_a	$(mmol\ N)^{-1}$	1.5
Zooplankton maximum growh rate	γ_z	d^{-1}	1.6
Zoop. ass. eff. feeding on P, B, D	β_p,β_b,β_d		0.75
Zoop. spec. excretion rate	ν_z	d^{-1}	0.1
Zoop. spec. mortality rate	μ_z	d^{-1}	0.01
Zoop. half-sat. for ingestion	K_z	$mmol\ N\ m^{-3}$	1.0
Detrital fraction of Zoop. mortality	d		0.33
Ammonium fraction of Zoop. excretion	a		0.75
Mnemiopsis maximum growh rate	γ_m	d^{-1}	2.0
Mnemiopsis ass. eff. feeding on Z	β_z		0.30
Mnemiopsis spec. mucus synt. rate	μ_u	d^{-1}	0.1
Mnemiopsis spec. excretion rate	ν_m	d^{-1}	0.1
Mnemiopsis spec. mortality rate	μ_m	$(mmol\ N\ m^{-3}d)^{-1}$	0.005
Detrital fraction of Zoop. mortality	d		0.33
Ammonium fraction of Zoop. excretion	a		0.75
Bacterial maximum growth rate	γ_b	d^{-1}	0.5
Bacterial specific excretion rate	ν_b	d^{-1}	0.05
Bacterial Half-sat.rate for uptake	K_b	$mmol\ N\ m^{-3}$	0.5
NH_4^+ / DON uptake ratio	η		0.6
Detrital breakdown rate	μ_d	d^{-1}	0.05
Detrital sinking rate	w_d	$m\ d^{-1}$	1.0

nitrate gradient were varied to determine sensitivity of the analyses to the choice of model and environmental parameters.

Allowing sub-pycnocline nutrient variations with respect to density produced better results compared to the case with constant nutrients. The slope and timing of mixed layer deepening in winter were critical in deter-

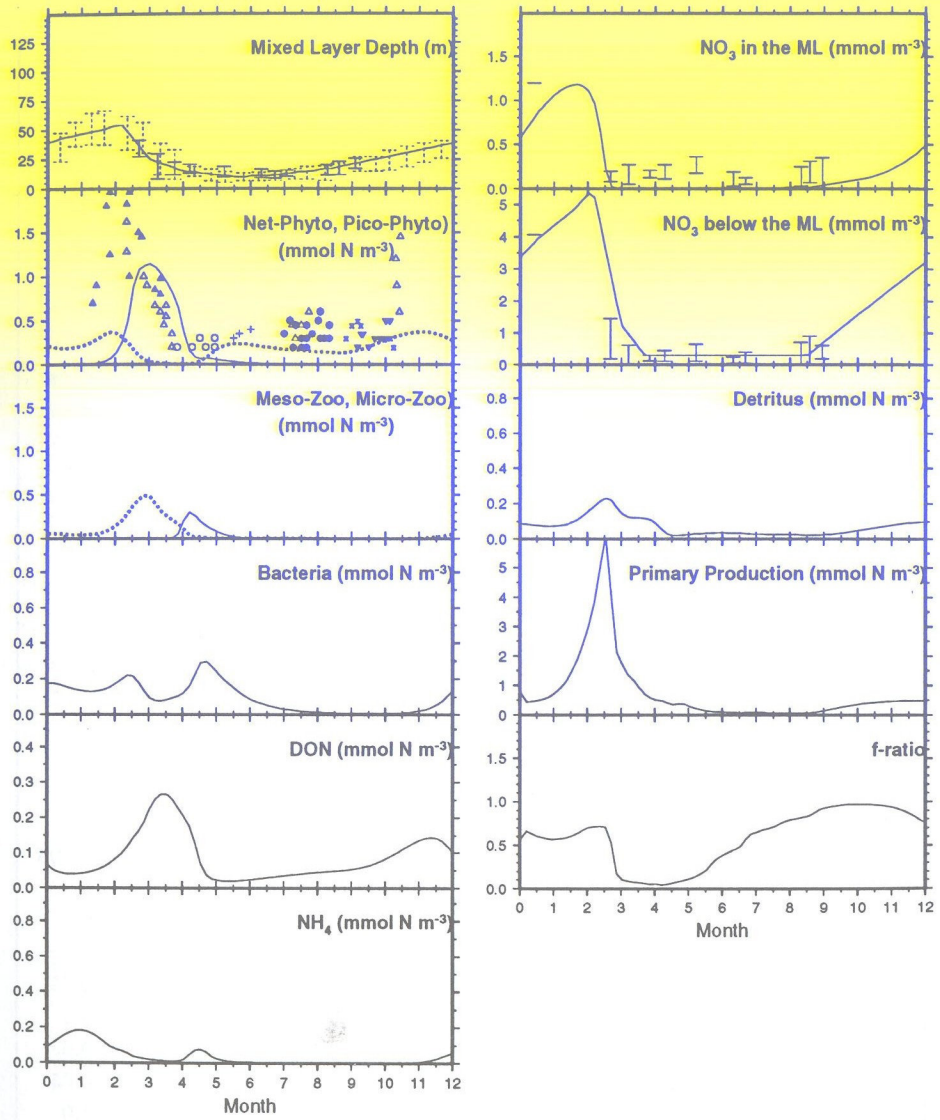


Figure 11. Results of the 9-compartment model run with values of constants in Table 5 for region 1 (dashed lines are pico phytoplankton and micro zooplankton.

mining model response (Figures 12a,b).

The phytoplankton bloom is depleted earlier when the sub-pycnocline NO_3 gradient S is increased ($S = 0.16$). Interestingly, the maximum phytoplankton concentration showed very little variation with S but the bloom was depleted about 15 days earlier, compared to the standard run, producing a small secondary peak (Figure 12c).

TABLE 5. 9-compartment model (2-phyto, 2-zoo) parameters

Parameter	*Symbol*	*Units*	*Value*
Mixed layer depth	h	m	
Diffusive mixing rate	m	$m\ d^{-1}$	0.1
PAR/total irradiance	-		0.41
Cloudiness	-	*oktas*	4
Light attenuation by water	k_w	m^{-1}	0.08
Net-phyto (P_1) max. growth rate	γ_{p1}	d^{-1}	2.5
Pico-phyto (P_2) max. growth rate	γ_{p2}	d^{-1}	1.5
Initial slope of $P-I$ curve for P_1	α_{p1}	$(W\ m^{-2})^{-1}d^{-1}$	0.025
Initial slope of $P-I$ curve for P_2	α_{p2}	$(W\ m^{-2})^{-1}d^{-1}$	0.013
Half-sat., for NO_3^- uptake by P_1	K_{pn1}	$mmol\ N\ m^{-3}$	0.5
Half-sat., for NH_4^+ uptake by P_1	K_{pa1}	$mmol\ N\ m^{-3}$	0.2
Half-sat., for NO_3^- uptake by P_2	K_{pn2}	$mmol\ N\ m^{-3}$	0.25
Half-sat., for NH_4^+ uptake by P_2	K_{pa2}	$mmol\ N\ m^{-3}$	0.2
P_1 Phytop. specific mortality rate	μ_p	d^{-1}	0.025
P_2 Phytop. specific mortality rate	μ_p	d^{-1}	0.02
Light atten. by phytoplankton	k_c	$m^2(mmol\ N)^{-1}$	0.02
Phytop. exudation fraction	e		0.05
NH_4^+ inhibition parameter	Ψ_a	$(mmol\ N)^{-1}$	1.5
Meso-zoo. (Z_1) max. growh rate	γ_{z1}	d^{-1}	2
Micro-zoo. (Z_2) max. growh rate	γ_{z2}	d^{-1}	1.2
Ass. eff., Z_1 feed. on P_1, Z_2, D	β_{p1z1}, β_{z2z1}, β_{dz2}		0.75
Ass. eff., Z_2 feed. on P_2, D	β_{p2z2} and β_{bz2}		0.75
Z_1 Zoop. spec. excretion rate	ν_{z1}	d^{-1}	0.1
Z_1 Zoop. spec. mortality rate	μ_{z1}	d^{-1}	0.04
Z_2 Zoop. spec. excretion rate	ν_{z2}	d^{-1}	0.01
Z_2 Zoop. spec. mortality rate	μ_{z2}	d^{-1}	0.035
Z_1 and Z_2 half-sat. for ingest.	K_z	$mmol\ N\ m^{-3}$	1.0
Detrital fraction of Z_1 mortality	d		0.33
Ammonium frac. of Z_1 excretion	a		0.75
Bacterial maximum growth rate	γ_b	d^{-1}	0.5
Bacterial spec. excretion rate	ν_b	d^{-1}	0.05
Bacterial Half-sat.rate for uptake	K_b	$mmol\ N\ m^{-3}$	0.5
NH_4^+ / DON uptake ratio	η		0.6
Detrital breakdown rate	μ_d	d^{-1}	0.05
Detrital sinking rate	w_d	$m\ d^{-1}$	1.0
P_2 phyto. sinking rate	w_{p2}	$m\ d^{-1}$	1

Although it is difficult to assign *a priori* values the cross-pycnocline mixing rate m, varying its values from 0.1 and 0.15 $m\ day^{-1}$ increased the

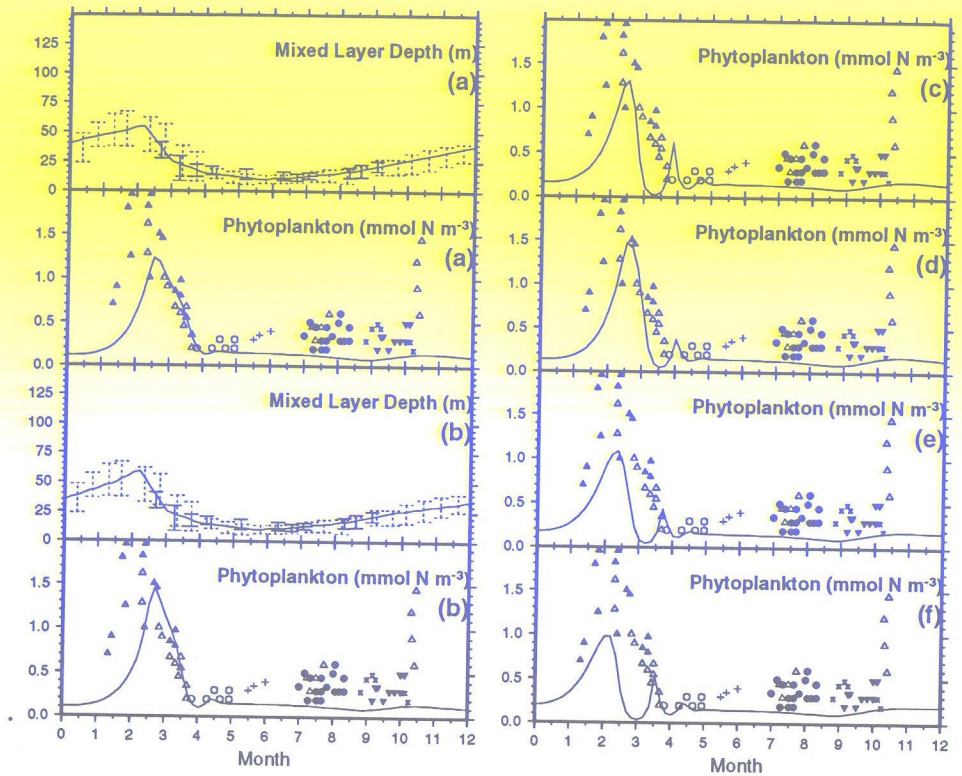


Figure 12. Results of the sensitivity analyses for the 7-compartment model, (a) run with values of constants in the first column of Table 1 for region 1, (b) increasing the time rate deepening of mixed layer (c) increasing the sub-mixed layer gradient of NO_3 ($S = 0.16$) (d) increasing the diffusive mixing rate ($m = 0.15\ m\ d^{-1}$) (e) increasing the initial slope of P-I curve, ($\alpha = 0.02\ (Wm^{-2})^{-1}\ d^{-1}$) (f) decreasing the water attenuation coefficient ($k_w = 0.06\ m^{-1}$). Open circles show the euphotic layer average chlorophyll concentrations ($mg\ Chl\ m^{-3}$). The data are redrawn from Vedernikov and Demidov (1993).

mixed layer NO_3 towards the observed levels, increasing the maximum of phytoplankton, but also causing the bloom to be depleted earlier (Figure 12d).

The model is very sensitive to photosynthesis and light parameters. The phytoplankton bloom occurs earlier by increasing the the initial slope of $P - I$ curve ($\alpha = 0.02\ (Wm^{-2})^{-1}\ d^{-1}$) (also resulting in an earlier grazing pressure by zooplankton, Evans and Parslow, 1985; Frost 1987), or decreasing the water attenuation coefficient ($k_w = 0.06\ m^{-1}$) (Figures 12e,f). The model is also very sensitive to maximum phytoplankton growth rate, γ_p.

7.3. REGIONAL ECOSYSTEMS

The specific seasonal variation of mixed layer depth in each of the model regions (Figure 4), resulting from local meteorological conditions, circulation and seawater properties, is specified in terms of average observations. The NO_3 concentration below the mixed layer, as influenced by mixed layer depth changes and biochemical cycling is also specified as input for the model. The values of k_w, γ_p, α, γ_z, characterizing each region were changed, keeping other parameters the same, to obtain results as close as possible to the available observations of average mixed layer chlorophyll-a or nutrients in the mixed layer.

7.3.1. *Region 1*

In Region 1, the onset of NO_3 occurs at greater density surfaces but relatively shallower depths with a sharp sub-pycnocline NO_3 gradient ompared to other regions. The sub-pycnocline NO_3 reaches 5.5 $mmol\ m^{-3}$ in winter, yielding 1.4 $mmol\ m^{-3}$ in the mixed layer. With a plankton bloom, confined to a narrow time interval coincides with data from Vedernikov and Demidov (1993). The annual mean of f-ratio is 0.65. It is around 0.7-0.8 from October till March as the heterotrophic stocks are low in this period. Thus f reaches to its minimum value as nutrient regeneration appears to be important in this system.

7.3.2. *Region 2*

The observed spring (March-May, Figure 2) or early summer (June-July, satellite observations, Sur *et al.*, 1994, 1996) phytoplankton blooms in the coastal parts of the Black Sea are more difficult to generate within the given parameter settings of the present model, unless lateral supply of nutrients by advected river water are not taken into account. This is because the observed concentrations of plankton in the peripheral region are much higher than those encountered in the central region (Figure 1). Without any lateral inputs the model results in Figure 13 show that the phytoplankton bloom in Region 2 (southwest Black Sea) occur in February-March, and the peak values are much smaller than the observed peak values of phytoplankton pigments (conversion value ~1, following Oğuz *et al.*, 1996) in the nearby area of the Bosphorus exit.

To account for lateral inputs of nutrients by advection along the coast, the nitrate equation was modified as

$$\frac{dN}{dt} = -\sigma_n P - \frac{(m + r^+(t))}{h}(N - N_{n0}) + c_1 \frac{Q}{hA} D_n$$

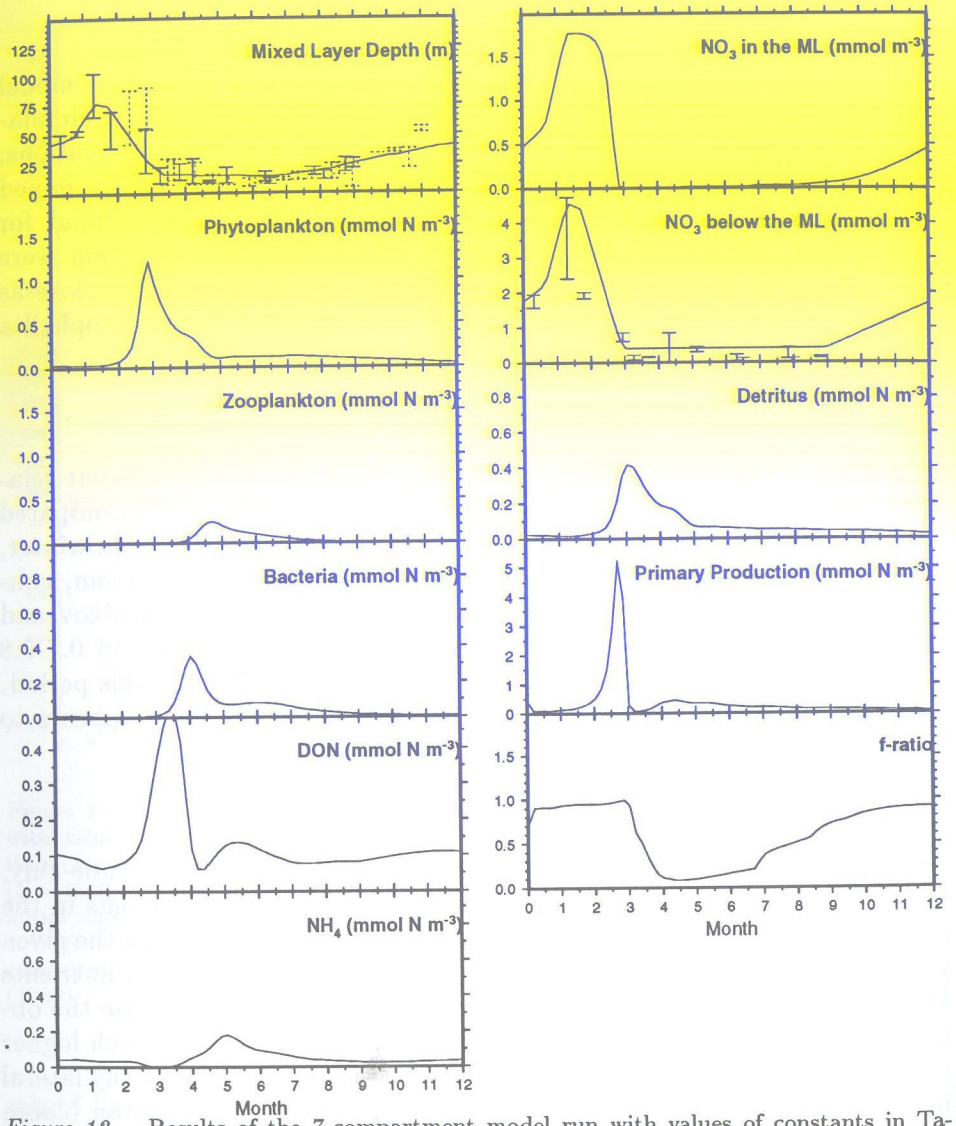


Figure 13. Results of the 7-compartment model run with values of constants in Table 1 for region 2. Bars show 95% confidence limits: solid bars, Bilim, HydroBlack and CoMSBlack cruises (1986-1995); dashed bars, Mamayev data (1926-1992).

where D_n, A, and Q denote respectively the Danube input, area considered, river flow rate, and c_1 is the fraction which defines the reduction of the Danube nitrates arriving in the region of interest.

The mean seasonal discharge of nutrients was estimated by multiplying the seasonal discharge and nutrient concentrations originating from the Danube (Cociasu *et al.*, 1996). We then assumed that a certain fraction of

these nutrients reaches the adjacent regions, advected by the rim-current. We distributed this source of nutrients uniformly over the area of the region within the surface layer.

In the case allowing for 15 % of Danube nutrients reaching Region 2 an increased bloom of phytoplankton continuing throughout the summer is created as a result of nutrients supplied by the spring flood of the Danube. The increased primary production and phytoplankton abundance in summer is nevertheless suppressed by zooplankton grazing.

A further increase of lateral nutrient supply (to 70 %) produces radical increases in phytoplankton (Figure 14), with peak values further shifted towards the summer, although it should be noted that some additional adjustments in parameters had to be made to obtain reasonable results. Although nutrients were available throughout the year, the intensive bloom occurrs as soon as the light availability increases in late spring.

With increased riverine nutrients, the separation between the phytoplankton peak and the zooplankton bloom is increased, and as a result, nutrients are depleted for a short time in summer (during the gap between phyto and zoo bloom peaks) by the massive phytoplankton bloom, when the primary production collapses. Note that, in this particular case μ_z is higher than the previous runs. It must be remembered that part of the zooplankton mortality is a model closure term representing the predation on zooplankton by higher predators which are not explicitely modelled. By comparing Figures 13 and 14, it can be seen that the time of maximum concentrations of phytoplankton, zooplankton, bacteria, DON, NH_4 are shifted about 2-3 months and increased 2-10 fold when the river input is taken into account.

7.3.3. *Region 3*

Intensive mixing is observed in this region between January and February months, causing influx of nutrients from the lower depths. The model produced the maximum NO_3 concentration below the mixed layer when the mixed layer depth was maximum (Figure 15). The bloom takes place in the beginning of March. The model results are very close to those for Region 1. However, NO_3 concentration in the mixed layer in February are higher than the observations. By increasing the initial slope of P-I curve ($\alpha = 0.06\ (Wm^{-2})^{-1}\ d^{-1}$), it becomes comparable with the observations, with a bloom occurring 15 days earlier than the previous run. In addition, the NH_4 concentration is obtained about 3 times higher than the previous case.

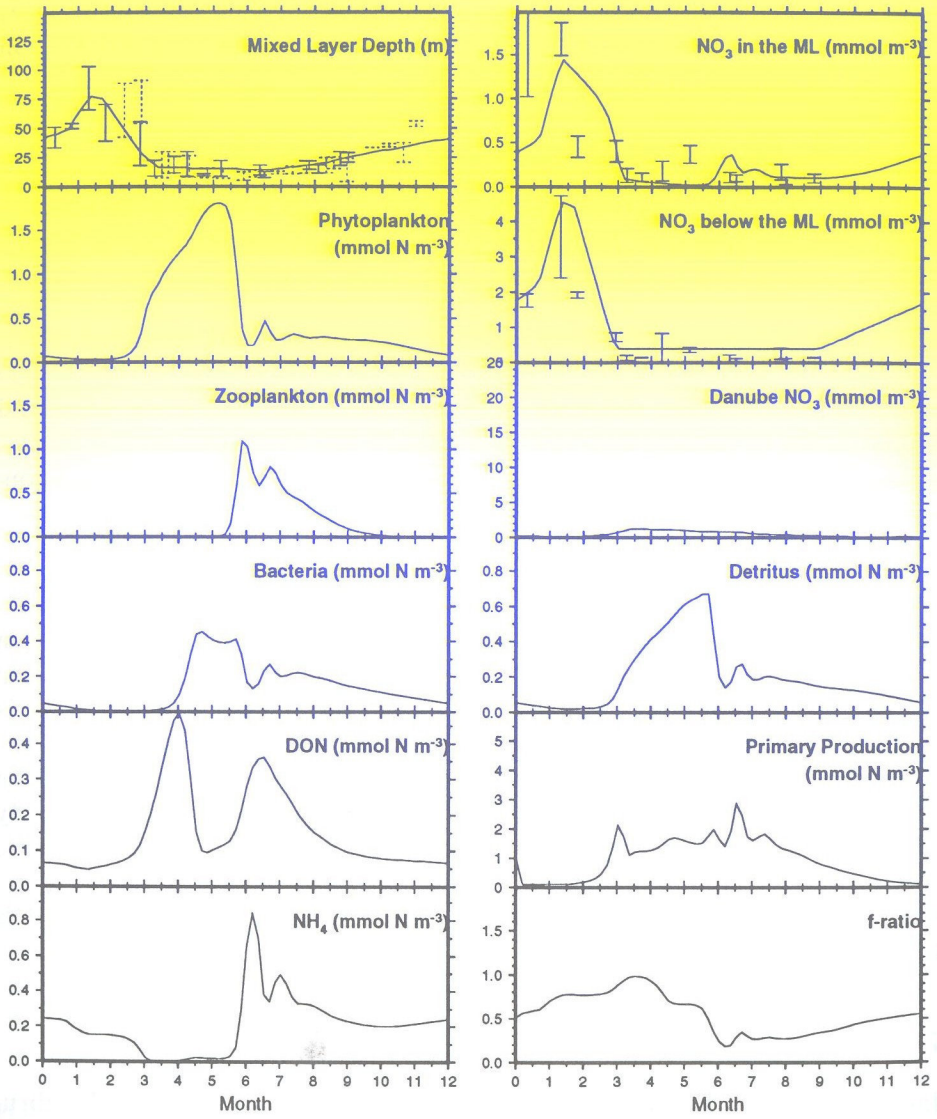


Figure 14. Results of the 7-compartment model run with values of constants in Table 1 for region 2 (except that $c_1 = 0.70$, $k_w = 0.12\ m^{-1}$, initial slope of P-I curve, $\alpha = 0.02\ (Wm^{-2})^{-1}\ d^{-1}$, zooplankton mortality, $\mu_z = 0.1\ d^{-1}$). Bars show 95% confidence limits: solid bars, Bilim, HydroBlack and CoMSBlack cruises (1986-1995); dashed bars, Mamayev data (1926-1992). Open circles show the mixed layer average chlorophyll concentrations ($mg\ Chl\ m^{-3}$) on K0 and B-15 stations.

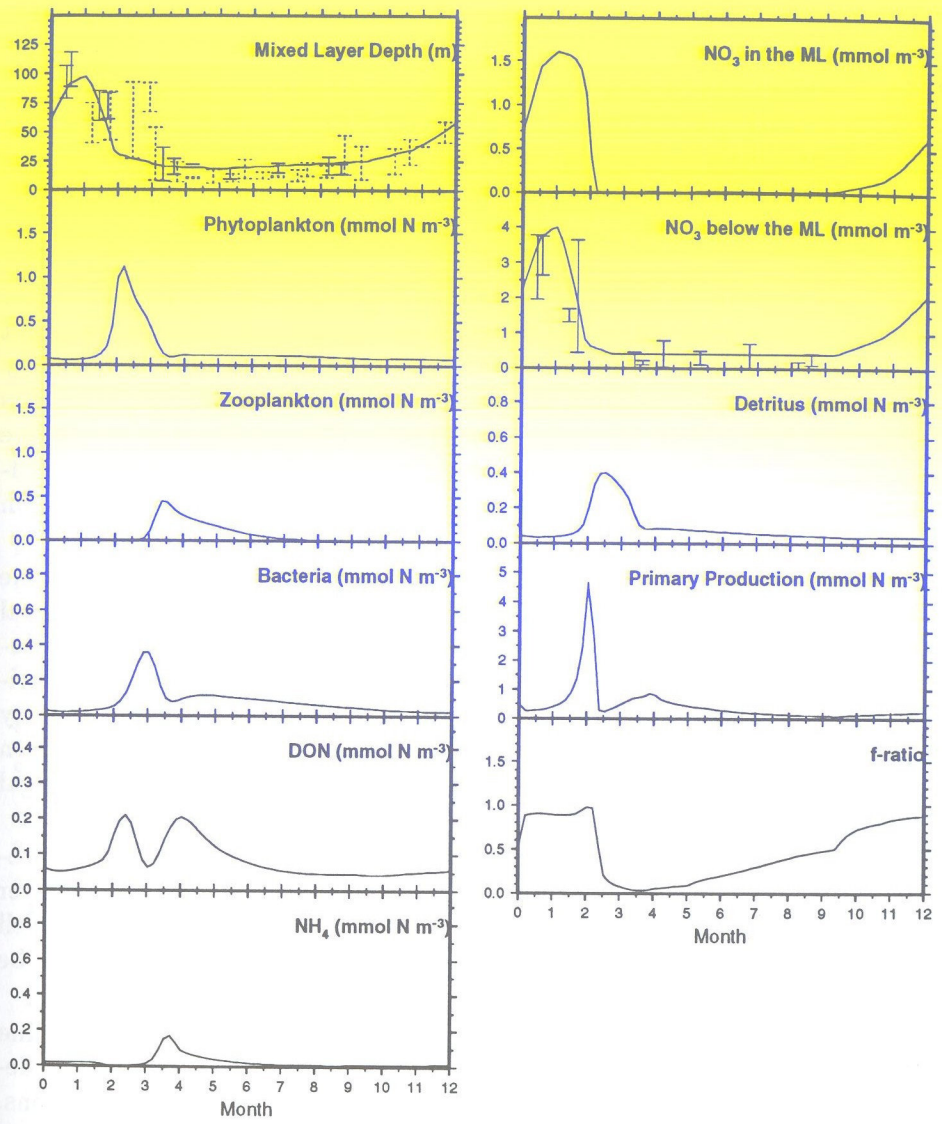


Figure 15. Results of the 7-compartment model run with values of constants in Table 1 for region 3. Bars show 95% confidence limits: solid bars, Bilim, HydroBlack and CoMSBlack cruises (1986-1995); dashed bars, Mamayev data (1926-1992).

7.3.4. *Region 10*

As noted earlier, the maximum phytoplankton concentration observed at the beginning of May was about 10-12 fold larger, compared with the central

region which is far from the effects of river inflow. The maximum of the model phytoplankton concentration roughly coincides with the observations if 45 % of the Danube flow is assumed to reach the Bosphorus (Figure 16). The phytoplankton bloom occurs in the April-June period coinciding with maximum Danube inflow and increased light availability.

8. Discussion and Conclusions

The large number of 'free' parameters in sophisticated ecosystem models, when combined with the lack of adequate environmental information to test the results, can limit the usefulness of modelling. Simple models guided by observations were considered in this study to guide and tune parameters for approaching closer to realistic estimates. The preliminary results are encouraging. Further studies are needed to test which one of these models leads to a better, yet simple approximation for the seasonal plankton dynamics as elaborated by observations in the Black Sea.

The comparison of model results with available data shows that some features of the model results are sufficiently realistic, such as the seasonal cycle of the nitrates in the mixed layer and the seasonal timing and duration of blooms. However, large uncertainties exist in estimating nutrients supplied to the coastal waters and their effects in sustaining primary production. The nutrient rich waters of the Danube reaching the western Anatolian coast near the Bosphorus appears to support enhanced algal production.

The differences in nitrate cycling between the regions are well reproduced in winter. The summer nutrient concentrations in the mixed layer obtained from the model are lower than most observations, but agree well with the R/V *Knorr* observations (Codispoti *et al.*, 1991), which may be relatively more accurate at the low concentrations measured.

Upwelling divergence resisting mixed layer deepening (greater nutricline gradient at higher density) in the cyclonic region seems to lead to an delayed bloom that is also depleted earlier as compared to the other regions. This is in agreement with the observations (*e.g.* Sur *et al.*, 1994, 1996). Zooplankton grazing is an important factor controlling the seasonal patterns. If the time lag between the phytoplankton and zooplankton blooms is increased, the magnitude of the zooplankton bloom and its NH_4 excretion are decreased.

The spring bloom in the central Black Sea and the Bosphorus region are reproduced well but the late autumn bloom observed in the central Black Sea is not evident in the 7 compartment model and is underestimated using the 9 compartment model including size groups.

The seasonal phytoplankton blooms in the peripheral regions of the

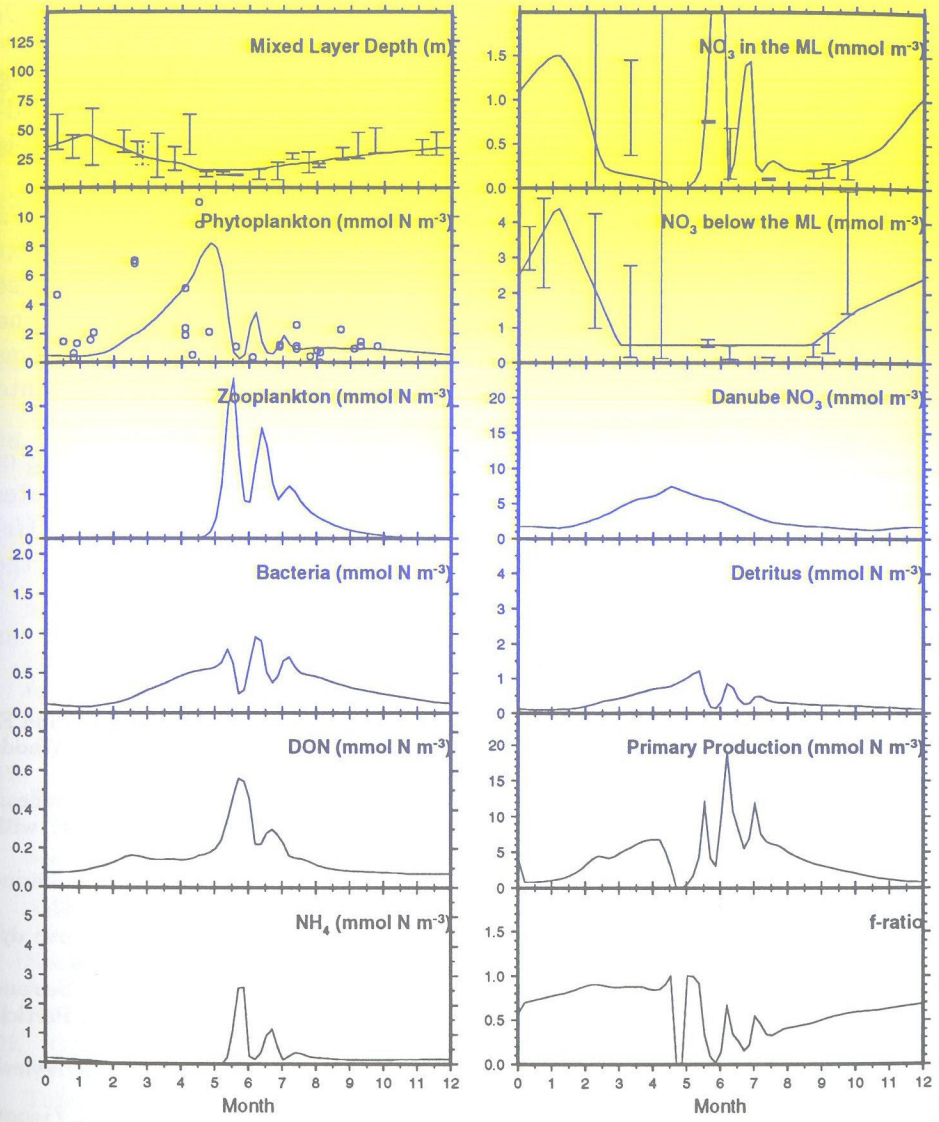


Figure 16. Results of the 7-compartment model run with values of constants in Table 1 for region 10 (except that $c_1 = 0.45$, $k_w = 0.14\ m^{-1}$, $\alpha = 0.02\ (Wm^{-2})^{-1}\ d^{-1}$, $\mu_z = 0.18\ d^{-1}$). Bars show 95% confidence limits: solid bars, Bilim, HydroBlack and CoMSBlack cruises (1986-1995); dashed bars, Mamayev data (1926-1992). Open circles show the mixed layer average chlorophyll concentrations ($mg\ Chl\ m^{-3}$) on KO and B-15 stations.

Black Sea, west Anatolian coast (region 2), Danube estuary (region 7a), Bosphorus (region 10), could only be reproduced reasonably well when nutrient advection from riverine sources was taken into account, emphasizing the importance of the Black Sea circulation. The obvious next level of modelling based on the present results is a network of regional ecosystem models must be coupled by fluxes of matter between them.

The highest phytoplankton concentrations were obtained in regions 2, 7a and 10. The central Black Sea and the south Anatolian coasts had the next highest phytoplankton concentrations. The phytoplankton bloom is intense in region 1 because of the higher diffusive mixing and the sharper nutricline gradient compared to the other regions. The highest mixed layer depth was observed in region 3, where the larger amounts of nutrients entrained into the mixed layer causes an intensive bloom.

Improvements in the present model can be obtained by (*i*) coupling of regional systems by interactive fluxes of matter, (*ii*) improving the estimates of the input by rivers (*iii*) including the atmospheric input of nutrients (*iv*) including more realistic nutrient limitation by including PO_4 and Si in the formulation of limitation.

References

1. Aubrey, D. G., Oğuz, T., Demirov, E., Ivanov, V., McSherry, T., Diaconu, V., and E. Nikolaenko. 1992b. HydroBlack 91: Report of the CTD Calibration Workshop, Woods Hole Oceanographic Institution, Report No: WHOI–92–10.
2. ASRSOMS (1996), Applications of Satellite Remote Sensing over the Mediterranean Sea, Brochure prepared by Satellite Observing Systems, Godalming, Surrey, UK, with support from EC (DGXII), ESA (ESRIN) and IOC, 80 pp.
3. Barale V. abd C. N. Murray (1995). The Surface Colour Field of Enclosed Marine Basins: Pigment Patterns of the Black Sea, *Remote Sensing Reviews*, **12**, 61-82.
4. Baştürk, Ö., Tugrul, S. and İ Salihoğlu (1996). Vertical chemistry of the three dynamically different regions of the Black Sea, *Turkish J. Mar. Sci.*, 2(1), 35-50.
5. Benli, H., (1987). Investigation of plankton distribution in the southern Black Sea and its effects on particle flux. In: E.T.Degens, E. Izdar and S. Honjo (Editors), Particle Flux in the Ocean. Mitt. Geol.-Paleontol., Univ. Hamburg, 62: 77-87.
6. Bologa, A.S., (1986). Planktonic primary productivity of the Black Sea: A review. Thalassia Jugosl., 22: 1-22.
7. Cociasu, A., Diaconu, V., Popa, L., Buga, L., Nae, I., Dorogan, L., V. Malciu (1996). The nutrient stock of the Romanian shelf of the Black Sea during the last three decades. in E. Özsoy and A. Mikaelyan (editors), *Sensitivity to Change: Black Sea, Baltic Sea and North Sea*, NATO ASI Series 2, Environment - **27**, Kluwer Academic Publishers, 1997, pp. 49-64.
8. Codispoti, L.A., Friederich G.E., Murray J.M., and Sakamoto C.M. (1991). Chemical variability in the Black Sea: Implications of continuaous vertical prifiles that penetrated the oxic/anoxic interface, *Deep Sea Res., Part A*,**38**, suppl., 2a, S691-S710, 1991.
9. Ducklow, H. W. and M. J. R. Fasham (1992). Bacteria in the Greenhouse: Modeling the Role of Oceanic Plankton in the Global Carbon Cycle, In: Mitchell, R., (editor), *Environmental Microbiology*, Wiley-Liss, New York, 1-31.
10. Eeckhout, D. V. and C. Lancelot (1996). Modelling the Functioning of the North-Western Black Sea Ecosystem from 1960 to Present, in E. Özsoy and A. Mikaelyan (editors), *Sensitivity to Change: Black Sea, Baltic Sea and North Sea*, NATO ASI Series 2, Environment - **27**, Kluwer Academic Publishers, 1997, pp. 455-468.
11. Evans, G. T. (1988). A Framework for Discussing Seasonal Succession and Coexistence of Phytoplankton Species, *Limnol. Oceanogr.*, **33**, 1037-1036.
12. Fasham, M. J. R., Ducklow, H. W. and S. M. McKelvie (1990). A Nitrogen-Based Model of Plankton Dynamics in the Oceanic Mixed Layer. *J. Mar. Res.* **48**, 591-639.
13. Fasham, M. J. R. (1994). Variations in the Seasonal Cycle of Biological production in Subarctic Oceans: A Model Sensitivity Analysis, 47 pp., 19 figs., *submitted to Deep-Sea Research.*
14. Frost B. W. (1987). Grazing control of phytoplankton stock in the subarctic Pacific: a model assessing the role of mesozooplankton, particularly the large calanoud copepods, Neocalanus spp. *Marine Ecology Progress Series*, **39**, 49-68.
15. Hay, B. J., Arthur, M. A., Dean, W. E. and E.D. Neff (1991). Sediment deposition in the Late Holocene abyssal black sea: Terrigenous and biogenic matter. *Deep-Sea Res.*, **38**(Suppl.), S711-S723.
16. Ivanov, L., Beşiktepe, Ş., Vladimirov, V. L., Latif, M. A., Oğuz, T., Konovalov, S., Salihoğlu, İ., Tuğrul, S., Romanov, A. and Ö. Baştürk. (1994). Report of the Physical and Chemical Intercalibration of the April-May 1994 Data (Joint TU-BLACK SEA and CoMSBlack Cruises), Institute of Marine Science, Middle East Technical University, Erdemli, İçel, Turkey.
17. Karl, D. M. and G. A. Knauer (1991). Microbial production and particle flux in the upper 350m of the Black Sea, *Deep-Sea Research*, **38(2A)**: 921-942.
18. Konovalov, S., Romanov, A., Salihoğlu, İ, Baştürk, Ö., Tuğrul, S. and S. Gökmen (1994). Intercalibration of CoMSBlack-93a Chemical Dta, Unification of Methods for Dissolved Oxygen and Hydrogen Sulfide Analyses and Sampling Strategies of CoMSBlack-94a Cruise, Institute of Marine Sciences, Middle East Technical University, Erdemli, İçel, Turkey, 26 pp.
19. Neuymin, G. G. (1980). Optical Properties of the Black Sea Waters, *The Complex Oceanographical Investigations of the Black Sea*, Kiev, Nauka Dumka, pp. 199-215.
20. Nezlin, N. P. (1997). Seasonal Variation of Surface Pigment Distribution in the Black Sea on CZCS Data, in E. Özsoy and A. Mikaelyan (editors), *Sensitivity to Change: Black Sea, Baltic Sea and North Sea*, NATO ASI Series 2, Environment - bf 27, Kluwer Academic Publishers, 1997, pp. 131-138.
21. Nierman, U., Bingel, F., Gorban, A., Gordina, A. D., Gücü, A., Kıdeyş, A. E., Konsulov, A., Radu, G., Subbotin, A. A. and V. E. Zaika (1993) Distribution of Anchovy Eggs and Larvae (*Engraulis encrasicolus* Cuv.) in the Black Sea in 1991 and 1992 in Comparison to Former Surveys, *ICES*, CM1993/H:48, 19p.
22. Oğuz, T., Beşiktepe, Ş., Baştürk, Ö., Salihoğlu, İ., Aubrey, D., Balcı, A., Demirov, E., Diaconu, V., Dorogan, L., Duman, M., Ivanov, L., Konovalov, S., Stayanov, S., Tuğrul, S., Vladimorov, V. and A. Yılmaz. (1993c). CoMSBlack'92a, Report on the Physical and Chemical Intercalibration Workshop, 15-29 January 1993, CoMSBlack 93-012 Technical Report, Institute of Marine Sciences, METU, Erdemli, Turkey, May 1993.
23. Oğuz, T., Latun, V. S., Latif, M. A., Vladimirov, V. V., Sur, H. I., Markov, A. A., Özsoy, E., Kotovshchikov, B. B., Eremeev, E. E. and Ü. Ünlüata. (1993). Circulation in the Surface and Intermediate Layers of the Black Sea. Deep-Sea Research, 40, 1597-1612.
24. Oğuz, T., Ducklow H., Malonotte-Rizzoli, P., Tuğrul, S., Nezlin, N. and Ü Ünlüata (1996). Simulation of annual plankton productivity cycle in the Black Sea by a one-dimensional physical -biological model, *Journal of Geophysical Research*, **101**, 16585-16599.
25. Sorokin, Y. I. (1983). The Black Sea, in: B. H. Ketchum (editor), *Estuaries and Enclosed Seas Ecosystem of the World*, pp. 253-292. Elsevier, New York.

26. Sukhanova, I. N., Flint, M. V., Hibaum, G., Karamfilov, V., Kopylov, A. I., Matveea, E., Rat'kova, T. N. and A. P. Sazhin (1988). Exuviaella cordata red tide in Bulgarian coastal waters (May to June 1986). *Mar. Biol.*, **99**: 1-8.
27. Sur, H. İ., Özsoy, E. and Ü. Ünlüata, (1994). Boundary Current Instabilities, Upwelling, Shelf Mixing and Eutrophication Processes In The Black Sea, *Prog. Oceanog.*, **33**, 249-302.
28. Sur, H.I., Özsoy, E., Ilyin, Y.P. and Ü. Ünlüata (1996). Coastal / Deep Ocean Interactions in the Black Sea and Their Ecological / Environmental Impacts. *Journal of Marine Systems*, 7, 293-320.
29. Trukhchev D. I. and R. A. Ibrayev (1997). Seasonal Variability of the Black Sea Climatic Circulation, in E. Özsoy and A. Mikaelyan (editors), *Sensitivity to Change: Black Sea, Baltic Sea and North Sea*, NATO ASI Series 2, Environment - **27**, Kluwer Academic Publishers, 1997, pp. 365-374.
30. Tuğrul, S., Baştürk, Ö., Saydam C. and A. Yılmaz (1992). Changes in the hydochemistry of the Black Sea inferred from density profiles, *Nature*, **359**,137-139.
31. Uysal, Z. and H. I. Sur (1995). Net Phytoplankton Discriminating Patches Along the Southern Black Sea Coast in Winter 1990, *Oceanologica Acta*, **18**, 639-647.
32. USGOFSO (1989). Ocean Color from Space, Mediterranean image, A folder of CZCS images prepared by NSF/NASA sponsored US Global Ocean Flux Study Office, Woods Hole Oceanographic Institution.
33. Vedernikov, V. I. and A. B. Demidov (1993). Primary production and chlorophyll in the deep regions of the Black Sea, *Oceanology.Engl.Transl.*,**33**, 193-199.
34. Vidal, C. V. (1995). Bio-Optical Characteristics of the Mediterranean and the Black Sea, M. Sc. Thesis, Institute of Marine Sciences, Middle East Technical University, Erdemli - İçel Turkey.
35. Vinogradov, M. Y. and E. A. Shushkina (1992). Temporal changes in community structure in the open Black Sea, *Oceanology, Engl.Transl.*, **32**, 485-491.

A. THE MODEL STRUCTURE AND EQUATIONS

A.1. MODEL EQUATIONS FOR 4 COMPARTMENTS

Model variables: P=phytoplankton, Z=zooplankton, D=detritus, N=nitrogen (replacing $N = B + N_n + N_a + N_d$ in the 7 Compartment Model).

$$\frac{dP}{dt} = (1-e)\sigma P - g_p Z - \mu_p P - \frac{(m + r^+(t))}{h} P$$

$$\frac{dZ}{dt} = \beta_p g_p Z + \beta_d g_d Z - \nu_z Z - \mu_z Z - \frac{r(t)}{h} Z$$

$$\frac{dN}{dt} = -(1-e)\sigma P + \nu_z Z + (1-d)\mu_z Z + \mu_d D - \frac{(m + r^+(t))}{h}(N - N_{n0})$$

$$\frac{dD}{dt} = (1-\beta_p) g_p Z - \beta_d g_d Z - \mu_d D + \mu_p P - \frac{(m + r^+(t) + w_d)}{h} D$$

B. Model Equations for 9 compartments including Mnemiopsis

Model variables: P=phytoplankton, Z=zooplankton, M=mnemiopsis, B=bacteria, N_n=nitrate (NO_3^-), N_a=ammonia (NH_4^+), N_d=dissolved organic nitrogen (DON), U=mucus, D=detritus.

$$\frac{dP}{dt} = (1-e)\sigma P - g_p Z - \mu_p P - \frac{(m + r^+(t))}{h} P$$

$$\frac{dZ}{dt} = \beta_p g_p Z + \beta_b g_b Z + \beta_d g_d Z - \nu_z Z - \mu_z Z - \gamma_z M - \frac{r(t)}{h} Z$$

$$\frac{dM}{dt} = \beta_z \gamma_m Z M - (\mu_u + \nu_m + \mu_m) M - \frac{r(t)}{h} M$$

$$\frac{dB}{dt} = u_{nd} B + u_{na} B + u_{mn} B + u_{muc} B - g_b Z - \nu_b B - \frac{(m + r^+(t))}{h} B$$

$$\frac{dN_d}{dt} = e\sigma P + \mu_d D + (1-a)\nu_z Z - u_{nd} B - \frac{(m + r^+(t))}{h} N_d$$

$$\frac{dN_a}{dt} = -\sigma_a P - u_{na} B + \nu_b B + (a\nu_z + (1-d)\mu_z) Z + \nu_m M - \frac{(m + r^+(t))}{h} N_a$$

$$\frac{dN_n}{dt} = -\sigma_n P - \frac{(m + r^+(t))}{h}(N_n - N_{n0})$$

$$\frac{dU}{dt} = \mu_u M - u_m B - \frac{(m + r^+(t))}{h} M$$

$$\frac{dD}{dt} = (1-\beta_p) g_p Z + (1-\beta_b) g_b Z - \beta_d g_d Z - \mu_d D + \mu_p P - \frac{(m + r^+(t) + w_d)}{h} D$$

C. Model Equations for 9 Compartments with plankton size speciation

Model variables: P_1=net-phytoplankton, P_2=pico-phytoplankton, Z_1=meso-zooplankton, Z_2=protozoa, B=bacteria, D=detritus, N_n=nitrate (NO_3^-), N_a=ammonia (NH_4^+), N_d=dissolved organic nitrogen (DON).

$$\frac{dP_1}{dt} = (1-e_{p1})\sigma_1 P_1 - g_{p1z1}Z_1 - \mu_{p1}P_1 - \frac{(m+r^+(t))}{h}P_1$$

$$\frac{dP_2}{dt} = (1-e_{p2})\sigma_2 P_2 - g_{p2z2}Z_2 - \mu_{p2}P_2 - \frac{(m+r^+(t)+w_{p2})}{h}P_2$$

$$\frac{dZ_1}{dt} = \beta_{p1z1}g_{p1z1}Z_1 + \beta_{z2z1}g_{z2z1}Z_1 + \beta_{dz1}g_{dz1}Z_1 - \nu_{z1}Z_1 - \mu_{z1}Z_1 - \frac{r(t)}{h}Z_1$$

$$\frac{dZ_2}{dt} = \beta_{p2z2}g_{p2z2}Z_2 + \beta_{bz2}g_{bz2}Z_2 - g_{z2z1}Z_1 + -\nu_{z2}Z_2 - \mu_{z2}Z_2 - \frac{r(t)}{h}Z_2$$

$$\frac{dB}{dt} = u_{nd}B + u_{na}B - g_{bz2}Z_2 - \nu_b B - \frac{(m+r^+(t))}{h}B$$

$$\frac{dN_d}{dt} = e_1\sigma_1 P_1 + e_2\sigma_2 P_2 + \mu_d D + (1-a)\nu_{z1}Z_1 + (1-a)\nu_{z2}Z_2 - u_{nd}B - \frac{(m+r^+(t))}{h}N_d$$

$$\frac{dN_a}{dt} = -\sigma_{a1}P_1 - \sigma_{a2}P_2 - u_{na}B + \nu_b B + a\nu_{z2}Z_2 + (a\nu_{z1} + (1-d)\mu_{z1})Z_1 - \frac{(m+r^+(t))}{h}N_a$$

$$\frac{dN_n}{dt} = -\sigma_{n1}P_1 - \sigma_{n2}P_2 - \frac{(m+r^+(t))}{h}(N_n - N_{n0})$$

$$\frac{dD}{dt} = (1-\beta_{p1z1})g_{p1z1}Z_1 + (1-\beta_{p2z2})g_{p2z2}Z_2(1-\beta_{z2z1})g_{z2z1}Z_1 + (1-\beta_{bz2})g_{bz2}Z_2 - \beta_{dz1}g_{dz1}Z_1 - \mu_d D + \mu_{p1}P_1 + \mu_{p2}P_2 + \mu_{z2}Z_2 - \frac{(m+r^+(t)+w_d)}{h}D$$

For each phytoplankton group P_i, $(i = 1, 2)$, the phytoplankton specific growth rate σ_i is

$$\sigma_i(t,h,N_n,N_a) = \sigma_{ni}(t,h,N_n,N_a) + \sigma_{ai}(t,h,N_a),$$
$$\sigma_{ni} = J_i(t,h)Q_{nni}(N_n,N_a), \quad \sigma_{ai} = J_i(t,h)Q_{nai}(N_a),$$

where the light limited growth rate $J_i(t,M)$, the nutrient limitation factors Q_{nni} for nitrate and Q_{nai} for ammonia, and the light integrals I_i corresponding to the particular photosynthesis-irradiance relationship $F_i(I)$ of i'th phytoplankton are given by

$$J_i(t,h) = 2\tfrac{1}{h}\int^{\tau}\int^{h} F_i(I_i)dzdt,$$
$$Q_{nni}(N_n,N_a) = \frac{N_n e^{-\Psi_a N_a}}{K_{pni}+N_n}, \quad Q_{nai}(N_a) = \frac{N_a}{K_{pai}+N_a},$$
$$I_i(z,t) = I_0(t)e^{-(k_w+k_{ci}P_i)z}, \quad F_i(I_i) = \frac{\gamma_{pi}\alpha_i I_i}{\sqrt{\gamma_{pi}^2+\alpha_i^2 I_i^2}}.$$

In this particular model, the meso-zooplankton Z_1 grazes on net-phytoplank P_1, protozoa Z_2 and detritus D. The protozoans Z_2 graze on pico-phytoplankto P_2 and bacteria B. The grazing rates of meso-zooplankton on net-phytoplankto and protozoans on pico-phytoplankton are defined by

$$g_{p1z1} = \frac{\gamma_{z1}r_{p1}P_1^2}{K_{z1}(r_{p1}P_1+r_{z2}Z_2+r_dD)+r_{p1}P_1^2+r_{z2}Z_2^2+r_dD^2},$$
$$g_{p2z2} = \frac{\gamma_{z2}r_{p2}P_2^2}{K_{z1}(r_{p2}P_2+r_bB)+r_{p2}P_2^2+r_bB^2},$$

and similarly for feeding on other food for each group.